Title: Conditional *Dystrophin* ablation in the skeletal muscle and brain causes profound effects on muscle function, neurobehavior, and extracellular matrix pathways

Muthukumar Karuppasamy[1], Katherine G. English[1], James R. Conner[2], Shelby N. Rorrer[1], Michael A. Lopez[1], David K. Crossman[3], Jodi R. Paul[4], Miguel A. Monreal-Gutierrez[5], Karen L. Gamble[4], Karyn A. Esser[4], Jeffrey J. Widrick[2], Louis M. Kunkel[2,6-9], and Matthew S. Alexander[1,10-12]

[1]Department of Pediatrics, Division of Neurology at the University of Alabama at Birmingham and Children's of Alabama, Birmingham, AL 35294

[2]Division of Genetics and Genomics, Boston Children's Hospital, Boston, MA 02115, USA

[3]Department of Genetics at the University of Alabama at Birmingham, Birmingham, AL 35294

[4]Department of Psychiatry and Behavioral Neurobiology, University of Alabama at Birmingham, Birmingham, AL 35294

[5]Department of Physiology and Aging, University of Florida, Gainesville, FL 32610, USA

[6]Department of Pediatrics, Harvard Medical School, Boston, MA 02115, USA

[7]The Stem Cell Program, Boston Children's Hospital, Boston, MA 02115, USA

[8]Harvard Stem Cell Institute, Cambridge, MA 02138, USA

[9]The Manton Center for Orphan Disease Research at Boston Children's Hospital, Boston, MA 02115, USA

[10]UAB Center for Exercise Medicine at the University of Alabama at Birmingham, Birmingham, AL, 35294

[11]UAB Civitan International Research Center (CIRC), at the University of Alabama at Birmingham, Birmingham, AL 35233

[12]UAB Center for Neurodegeneration and Experimental Therapeutics (CNET), Birmingham, AL 35294, USA

Word Count: 5,911
Character Count: 34,988

Correspondence should be directed to:
Matthew S. Alexander, PhD
University of Alabama at Birmingham and Children's of Alabama
1900 University Blvd. THT 929 Box 96
Birmingham, AL 35294
Email for correspondence: matthewalexander@uabmc.edu

ORCID IDs:

Muthukumar Karuppasamy: 0000-0003-0034-9950

Katherine G. English: 0000-0003-2757-5157

James R. Conner: 0000-0002-8886-1475

Shelby N. Rorrer: 0009-0009-5640-9669

Michael A. Lopez: 0000-0002-3029-0761

David K. Crossman: 0000-0002-0981-169X

Jodi R. Paul: 0000-0002-5409-5944

Miguel A. Monreal-Gutierrez: 0000-0001-8601-4080

Karen L. Gamble: 0000-0003-3813-8577

Karyn A. Esser: 0000-0002-5791-1441

Jeffrey J. Widrick: 0000-0002-5597-1141

Louis M. Kunkel: 0000-0001-6126-0242

Matthew S. Alexander: 0000-0001-7406-5171

Author Contributions: M.K., K.G.E., J.R.C., J.R.P, M.A.M-G., S.N.R., D.K.C., and J.J.W. all performed experiments for the manuscript. M.A.L. and L.M.K. contributed key resources for the manuscript. M.K. M.A.L., K.L.G., K.A.E., J.J.W., and M.S.A. wrote the manuscript. All authors approved of the manuscript prior to its submission.

Competing Interest Statement: L.M.K is a consultant for Pfizer, Dyne Therapeutics, and Myofinity for muscle disease drug therapies. All other authors declare no conflicts of interest.

Classification: Medical Sciences

Keywords: Dystrophin, DMD, muscular dystrophy, skeletal muscle, Dystrophinopathy

Abstract

Duchenne muscular dystrophy (DMD) patients suffer from skeletal and cardiopulmonary weakness, and interestingly up to one third are diagnosed on the autism spectrum. Dystrophin is an essential protein for regulating the transmission of intracellular force to the extracellular matrix within the skeletal muscle, but also plays key roles in neurobehavior and cognitive function. The mouse dystrophin gene (also abbreviated *Dmd*) is X-linked and has several isoforms with tissue-specific expression, including the large *Dp427m* muscle transcript found in heart and skeletal muscle, and the *Dp427c* transcript that encodes the brain-specific dystrophin cerebellar protein. Understanding the functional requirements and pathways that are affected by dystrophin loss will impact dystrophin replacement gene therapy and exon-skipping correction strategies. We generated conditional *Dystrophin* knockout mice by targeting exon 52 of the mouse *Dystrophin* (*Dmd*^{flox52}) locus. We generated dystrophin constitutive and inducible myofiber knockout (*Dmd* mKO) mice to evaluate the tissue-specific function of the large skeletal muscle dystrophin isoform. Constitutive embryonic deletion of the *Dystrophin* gene exclusively in skeletal myofibers resulted in a severe skeletal muscle myopathy, dystrophic histopathology, and functional deficits compared to the *mdx* mouse. Transcriptomic analysis of skeletal myofibers of the *Dmd* mKO mice revealed the dysregulation of key extracellular matrix and cytokine signaling pathways. Separately, we generated Purkinje neuron cerebellar dystrophin knockout (*Dmd*:Pcp2 KO) mice that displayed neurobehavioral deficits in social approach, social memory, and spatial navigation and working memory. These studies reveal the essential requirement for dystrophin expression in both the skeletal muscle and brain for normal physiological and neurobehavioral function.

Significance Statement

Duchenne muscular dystrophy is caused by the lack of a functional dystrophin protein in muscle. The large dystrophin (Dp427m) isoform is expressed in skeletal, cardiac, and smooth muscle, but its tissue-specific requirements remain unknown. We generated and characterized a conditional skeletal muscle knockout mouse (*Dmd* mKO). Constitutive embryonic genetic ablation of skeletal muscle *Dystrophin* resulted in muscle histopathologies similar to the *mdx* mouse, while postnatal muscle *Dystrophin* ablation resulted in milder pathologies. Ablating cerebellar *Dystrophin* Dp427c using a *Pcp2/L7*-Cre driver resulted in sociobehavioral defects. Transcriptomic analysis of the *Dmd* mKO mice showed a severe reduction of extracellular matrix and cytokine signaling

121 pathways. Our study reveals an essential role for skeletal muscle dystrophin and identifies
122 essential pathways for modulation using dystrophin-replacement therapies.
123
124 **Introduction**
125 In Duchenne muscular dystrophy (DMD) patients there is a disruption of the dystrophin gene (also
126 abbreviated *DMD*) that is predominantly expressed in skeletal and cardiac muscle. DMD patients
127 develop progressive muscle weakness in their teenage years that results in severe muscle
128 degeneration and cardiorespiratory complications. The *DMD* gene is X-linked, thus DMD
129 predominantly affects males who lose the ability to walk by their early teenage years. Mammalian
130 dystrophin protein is an essential protein that is required for normal skeletal muscle function
131 through its key binding to the actin cytoskeleton and dystrophin-associated protein complex
132 (DAPC). When fully sequenced, the human *DMD* locus was found to be extremely large as it
133 spans 2.2 megabases (Mbs) and has multiple coding regions that are essential for the function of
134 the dystrophin protein(1). The regulation of the dystrophin protein is complex in that the major
135 protein (Dp427) is expressed in multiple tissues and organs including skeletal muscle, heart, lung,
136 intestine, and the brain(2). Further complexity of dystrophin transcriptional regulation exists in that
137 multiple isoforms and *DMD* promotors exist and the regulation of its expression on a tissue-
138 specific manner has yet to be fully elucidated.
139
140 The most widely used Duchenne mouse model is the *mdx* mouse, which harbors an *Dmd* exon
141 23 nonsense mutation (C>T) at nucleotide 3185 of the large *Dp427m* RNA transcript(3, 4). Several
142 other N-ethyl-N-nitrosourea (ENU) mutagenesis and targeted knockout mouse strains have been
143 generated since the identification of the *mdx* mouse, that all show varying muscle phenotypes
144 based on the DMD mutation type and *Dystrophin* exon(s) targeted(5). Additional DMD mouse and
145 other animal models have been generated and assessed for their dystrophin expression, mutation
146 location, muscle pathophysiologies, and their ability to respond to pre-clinical and clinical
147 corrective drugs. Attempts to generate conditional mouse models have had mixed outcomes due
148 the large *DMD* gene loci and difficulties in targeting the X chromosome using gene editing. One
149 study demonstrated that a dual *Dmd* exon 2 and 79 floxed mouse when mated with a tamoxifen-
150 inducible cardiac and skeletal muscle *MerCreMer* transgene resulted in 25-35% dystrophin gene
151 excision(6). A previously homologous recombination (HR)-established knockout mouse targeting
152 dystrophin exon 52 (a known DMD mutation “hot spot” region) resulted in the disruption of the
153 large Dp427, Dp260, and Dp140 dystrophin isoforms(7). This dystrophin exon 52 model (*mdx52*)
154 displayed severe muscle degeneration pathologies, in addition to cardiac and neurobehavioral

155 defects similar to those observed in the *mdx* (*Dmd* exon 23) mouse(7-10). More in-depth
156 comparisons of multiple DMD mouse strains have revealed neurological, cognitive, and
157 behavioral deficits compared to WT controls(11, 12). Using this knowledge, we generated a
158 conditional-ready *Dmd* mouse by inserting loxP sites flanking *Dystrophin* exon 52 (Dmd^{flox52}) that
159 allowed for the ablation of the large *Dp427* isoforms upon Cre-mediated excision. Combinatorial
160 mating with skeletal myofiber Cre lines allowed us to define the tissue-specific requirements of
161 the dystrophin protein in skeletal muscle in early and post-natal muscle growth and regeneration.
162 Separate matings with a Purkinje neuronal Cre line also recapitulated several of the learning,
163 cognitive, and social deficits as other DMD mouse lines.
164
165 **Results**
166 ***Generation and initial characterization of skeletal muscle Dystrophin knockout mice***
167 We performed CRISPR-targeting of the mouse *Dystrophin* exon 52 locus and inserted two loxP
168 sequences in the intronic region immediately flanking the exon (**Figure 1A**). Upon Cre-mediated
169 excision of *Dmd* exon 52, the resulting DNA sequence contains an out-of-frame deletion that
170 impairs the stability of the Dp427, Dp260, and Dp140 transcripts as has been previously shown
171 in the *mdx52* mouse(13). We mated male $Dmd^{flox52/Y}$ mice with the constitutive human skeletal
172 actin (*HSA*)-Cre to ablate expression of the large Dp427m protein within the skeletal myofibers
173 (**Figure 1B**). We compared our conditional dystrophin knockout mouse model to the mdx^{5cv}
174 mouse that has well-characterized dystrophic histological, molecular, and physiological muscle
175 symptoms(14). The resulting $Dmd^{flox52/Y}$:HSA-Cre+ (*Dmd*:HSA KO) mice have no overt
176 pathologies at birth, but similar to many *mdx* strains develop a progressive muscle degeneration
177 starting between 4-6 months of age (**Figure 1C**). Analysis of both fast twitch *Tibialis anterior* (TA)
178 and slow twitch (soleus) muscles from *Dmd*:HSA KO mice showed increased centralized
179 myonuclei, large areas of fibrosis, and increased collagen production throughout the myofibers
180 (**Figure 1C**). *Dmd*:HSA KO diaphragm muscle also revealed hallmark muscle degeneration,
181 increased centralized myonuclei, and the presence of collagen deposits compared to Cre-
182 controls (**Figure 1C**). Cross-sectional area (CSA) of *Dmd*:HSA KO TA myofibers showed an
183 increased frequency of smaller myofibers compared to Cre- controls and similar to those found in
184 our mdx^{5cv} mice (**Figures 1D and 1E**). Quantitative western blot assessments of Dp427m protein
185 levels in the *Dmd*:HSA KO TA and soleus muscles showed an average of <5% remaining Dp427m
186 protein in the TA and the soleus muscles (**Figure 1F**). This was further confirmed using

immunofluorescent antibody staining in these muscles showing severely reduced levels of the large Dp427m protein (**Supplemental Figure S1**).

Skeletal myofiber loss of muscle dystrophin greatly impairs muscle physiological function

We performed a muscle functional analysis of the *Dmd*:HSA KO adult mice by performing an assessment of muscle performance following TREAT-NMD standard operating procedures (SOPs) for *mdx* mice(15). *Dmd*:HSA KO mice showed reduced rotarod latency to fall, open field test (OFT) total distance travelled, and impaired forelimb grip strength (**Figures 2A-2C**). All of these locomotor and muscle strength metrics were comparable to those of aged-matched *mdx* mice. *Dystrophin*-deficient mice have impaired treadmill running performance due in part to the lack of sarcolemma-associated neuronal NOS (nNOS) binding to Dp427 at the spectrin-like repeats encoded by *Dmd* exons 45-48(16, 17). We performed a standardized treadmill downhill running assessment of age-matched male WT, mdx^{5cv}, $Dmd^{flox52/Y}$ (Cre negative), and *Dmd*:HSA KO mice. The *Dmd*:HSA KO and mdx^{5cv} mice performed similarly in showing quicker times to exhaustion, reduced overall distance travelled, and reduced velocity compared to internal cohort control mice (**Figures 2D-2F**). These findings are consistent with the requirement of nNOS-binding to skeletal muscle dystrophin as essential for skeletal muscle exercise and running performance(18, 19). We assessed physiological force in EDL muscles from our *Dmd*:HSA KO mice to determine if there were functional deficits in the peak force and resistance to high mechanical strain. Despite their greater mass (**Supplemental Figure S2A**), EDL muscles from the *Dmd*:HSA KO mice attained similar peak force as EDL's from the $Dmd^{flox52/Y}$ Cre- controls (**Supplemental Figure S2B**). This reduction in force per unit physiological cross-sectional area of muscle (**Supplemental Figure S2C**) indicates a reduction in the quality of the *Dmd*:HSA KO EDL. Eccentric contractions reduced force of muscles from both groups of mice but this response was exacerbated in the *Dmd*:HSA KO mice (**Supplemental Figures S2D and S2E**). These results suggest that skeletal muscle Dystrophin loss has a moderate reduction in myofiber force output and resistance to mechanical strain in comparison with that of *mdx* mice.

***Dystrophin* myofiber KO mice have impaired skeletal muscle regeneration following injury**

We performed a cardiotoxin (ctx)-induced injury to the TA muscles of the *Dmd*:HSA KO and control $Dmd^{flox52/Y}$ mice to evaluate the regenerative capacity of the skeletal muscle in the absence of the Dp427m protein. The *Dmd*:HSA KO mice showed a significant amount of fibrosis, collagen, and necrotic regions within the muscle that was comparable to the mdx^{5cv} strain (**Supplemental Figure S3A**). Immunofluorescent analysis of the myofibers from the *Dmd*:HSA KO mice showed

221 elevated levels of centralized myonuclei after 21 days post ctx-injury (**Supplemental Figure**
222 **S3B**). These results demonstrate the absolute requirement for the dystrophin protein in the
223 myofiber and suggest that dystrophin from the muscle satellite cells (MuSCs) cannot compensate
224 for the lack of myofiber dystrophin in the normal regenerative process.
225
226 **Skeletal muscle-specific *Dystrophin* loss results in cytokine and ECM pathway disruption**
227 We performed RNA-sequencing on the *Dmd*:HSA KO and Cre- control TA muscles to determine
228 what transcript and signaling pathways were disrupted upon the loss of skeletal muscle
229 *Dystrophin* (**Figure 3A**). Ingenuity Pathway Analysis of RNA transcripts revealed several
230 inflammatory cytokine transcripts that were disrupted as well as extracellular matrix (ECM)
231 including several *Collagen* isoforms (**Supplemental Figure S4**). Interestingly, several transcripts
232 known to be disrupted in DMD patients were also disrupted in the *Dmd* HSA KO mice including
233 an elevation of inducible nitric oxide synthase 2 *(iNos*; *Nos2*) (**Figure 3D**). We noted a strong
234 downregulation in key immune-responsive cytokines including *Tgfb1* which drives DMD muscle
235 pathologies in *Dmd* HSA KO mouse muscles and indicates disruption of key cell-cell signaling
236 between the skeletal myofibers and the immune cells residing in the muscle (**Figures 3B-3D**).
237 These transcriptomic analysis confirms and delineates an essential transcriptomic regulation of
238 key signaling pathways that are known regulators of dystrophin pathophysiology.
239
240 **Postnatal skeletal myofiber *Dystrophin* loss impairs muscle maintenance despite**
241 **dystrophin protein stability**
242 We next sought to evaluate the role of skeletal muscle dystrophin in the regulation of adult skeletal
243 muscle maintenance and regeneration. Subsequently, we mated our conditional $Dmd^{flox52/Y}$ mice
244 to the *HSA*-MerCreMer tamoxifen-inducible skeletal myofiber Cre line to temporally ablate
245 Dp427m expression in the adult mice (**Figure 4A**). Two months after tamoxifen dosing, we
246 observed 25-30% reduction of total Dp427m protein within the TA skeletal muscles of *Dmd*:HSA-
247 MerCreMer+ (+ Tam) of *Dmd*:HSA-MerCreMer+ (-Tam) controls (**Figure 4B**). We observed a
248 similar 20-30% decrease of total Dp427m protein within the gastrocnemius and soleus muscles
249 in the *Dmd*:HSA-MerCreMer+ (+ Tam) mice (**Figure 4B**). These results are similar to the other
250 reported conditional *Dmd* mice that showed partial reduction of Dp427mprotein and highlights the
251 stability of the large dystrophin protein after 2 months of protein turnover(6). A histological
252 examination of the *Dmd*:HSA-MerCreMer+ (+ Tam) mice showed minimal myofiber degradation
253 and small pockets of regenerating myofibers compared to controls (**Figure 4C**). Overall myofiber
254 cross-sectional area (CSA) and minimal Feret diameter analysis revealed smaller clusters of

255 myofibers in the *Dmd*:HSA-MerCreMer+ (+ Tam) mice compared to no tamoxifen mock controls
256 (**Figures 4D and 4E**). These findings implicate the large amount of stability of the large dystrophin
257 Dp427m protein and implicate protein turnover as an essential part of dystrophin-restoration
258 therapies.
259

260 **Loss of cerebellar dystrophin impairs neurobehavioral function and results in ASD-like**
261 **behaviors**

262 Previous studies from our lab and others in various *mdx* strains demonstrated that the Dp427
263 cerebellar dystrophin isoform was essential for normal neurobehavior and social development(12,
264 20-22). We mated the conditional $Dmd^{flox52/Y}$ mice to *L7/Pcp2*-Cre (*Dmd*:Pcp2 KO) mice to ablate
265 the Dp427c protein in Purkinje neurons of the cerebellum (**Figure 5A**). Isolated cerebellums from
266 adult *Dmd*:Pcp2 KO mice showed loss of approximately 65% of cerebellar dystrophin protein
267 compared to Cre- controls (**Figure 5B**; **Supplemental Figure S5**). We performed a series of
268 neurobehavioral assessments in the *Dmd*:Pcp2 KO mice including social approach and social
269 novelty between novel and familiar objects and mice (**Figure 5C**). *Dmd*:Pcp2 KO showed
270 impaired social novelty in object recognition compared to $Dmd^{flox52/Y}$ Cre- control mice (**Figures**
271 **5D and 5E**). We performed a similar 3-chamber assessment (novel mouse versus familiar mouse)
272 and the *Dmd*:Pcp2 KO mice showed no preference for either mouse as compared to controls
273 suggesting that social behavior defects are linked to cerebellar dystrophin protein expression. We
274 performed both T- and Y-maze assessments in the *Dmd*:Pcp2 KO mice and found no differences
275 in T-maze alternations compared to Cre- control mice (**Figure 5F**). However, in the Y-maze
276 assessment, *Dmd*:Pcp2 KO mice had reduced alternations without a change in total arm visits
277 which together suggest reduced spatial working memory compared to Cre- controls (**Figure 5G**).
278 Memory tests were also conducted on the *Dmd*:Pcp2 KO mice that displayed impaired time to
279 find the platform in Morris water maze (**Figure 5H**). These findings support an essential role for
280 cerebellar Purkinje neuronal expression of *Dystrophin* and demonstrate a functional role for
281 Dp427 in the regulation of neurobehavior in DMD.
282

283 **Discussion**

284 The generation of novel DMD animal models using CRISPR gene editing and other next-
285 generation genomic DNA editing tools highlights the growing need for comprehensive animal
286 models that accurately reflect disease symptoms and pathophysiologies(23). Our conditional
287 dystrophin knockout model allows for the tissue-specific study of the impact of both dystrophin
288 loss and when combined with dystrophin-replacement strategies, correct DMD strategies. Newer

289 dystrophinopathy mouse models have identified the impact of dystrophin loss on muscle disease
290 symptom progression. The *bmx* (Becker muscular dystrophy; *Dmd* exons 45-47 in-frame deletion)
291 mouse has been useful in elucidating the slower muscle disease progression that occurs in
292 patients(24). Our conditional approach allows for the exploration of dystrophin requirements at
293 key developmental and DMD disease-relevant time points.
294
295 Previous attempts to delineate skeletal muscle dystrophin protein expression using AAV-shRNAi
296 strategies have revealed dystrophin as essential for sarcomeric organization within the muscle
297 myofiber(25). A study of cultured *mdx* mouse myoblasts revealed a similar downregulation of
298 Collagen and histone transcripts along with impaired fusion and proliferation markers(26). Indeed,
299 there may be a significant amount of epigenetic remodeling that occurs which was shown in
300 embryonic stem (ES) cell cultures of *mdx* mice and human induced pluripotent stem cells
301 (hiPSCs)(27, 28). Given the alteration of myogenic determinant transcriptional pathways,
302 consideration of the impact of *Dystrophin* loss on epigenetic influences on myogenic
303 differentiation is warranted(29). Key autophagy and PTEN/AKT pathways have been shown to be
304 targets for therapeutic amelioration of dystrophic muscle pathologies(30-32). Questions remain
305 on the impact and influence of the large dystrophin muscle isoform on muscle satellite cells
306 (MuSCs) and its regulation of cellular polarity(33, 34). The Dp427 protein is expressed in muscle
307 satellite cells and it is currently unclear if restoration of dystrophin expression in the MuSC
308 population could compensate for myofiber dystrophin loss. Therapies to restore MuSC polarity in
309 DMD MuSCs may be beneficial for restoring the cellular kinetics and polarity defects observed in
310 DMD muscles(35, 36).
311
312 It is evident that the expression of dystrophin protein does occur in the brain and both large and
313 smaller dystrophin isoforms likely play independent and critical neuronal functions. Clinical studies
314 have demonstrated that loss of dystrophin is important for normal neurological and
315 neurobehavioral function as up to one-third of all DMD patients are diagnosed on the ASD
316 spectrum with symptoms ranging from mild cognitive impairment to severe developmental
317 delay(11, 37-39). Evaluation of DMD mouse models have shown impaired neurobehavioral
318 responses in memory, learning, and overall electrophysiological neuronal function(22, 40-42). Our
319 *Dmd*:Pcp2 KO mice show similar defects to those in *mdx* mice, and highlight the essential role for
320 the large brain dystrophin protein expression. These results argue that newer platforms for exon-
321 skipping drug compounds that can more effectively penetrate the blood-brain-barrier (BBB) may
322 be required for the systemic restoration of dystrophin expression(43, 44). Our study demonstrates

323 the absolute requirement for dystrophin expression within the skeletal muscle and brain and
324 warrants further evaluation of the tissue-specific pathways impacted by dystrophin loss.
325 Elucidation of these dystrophin-regulated pathways will aide in dystrophin-replacement and
326 correction therapeutic strategies focused on the amelioration of DMD disease pathologies.
327

328 **Materials and Methods**

329 **Mice:**

330 Wild type (*C57BL/6J*; strain #000664; Jackson Labs) and *mdx*^{5cv} (*C57BL/6J*; strain #002379;
331 Jackson Labs) used in all experiments were maintained in the Alexander lab colony under
332 pathogen-free conditions. Constitutive HSA-Cre (*Acta1*-Cre; strain# 006149) and tamoxifen-
333 inducible *HSA-MerCreMer* (*HSA*-MCM; strain# 031934) were purchased from Jackson Labs (Bar
334 Harbor, ME) and maintained on a congenic *C57BL/6J* background. The *L7/Pcp2*-Cre mice were
335 originally purchased from Jackson Labs and maintained on a congenic *C57BL/6J* background
336 that had been backcrossed greater than 6 generations (strain #006207; Jackson Labs). All mice
337 had a standard Teklad Global Rodent Diet (Inotiv; West Lafayette, IN) with *ad libitum* access to
338 food and water. All mouse strains and protocols were approved by the UAB Institutional Animal
339 Care and Use Committee (IACUC) under the protocol 21393.
340

341 **Generation of conditional Dystrophin knockout mice:**

342 Conditional *Dystrophin* knockout mice *(Dmd*$^{flox52/Y}$) were generated commercially (Cyagen; Santa
343 Clara, CA) via CRISPR guide editing of genomic DNA by inserting loxP sites in the intronic regions
344 flanking mouse *Dystrophin* exon 52 using a 12.2 kb homologous recombination vector. Briefly,
345 loxP sequences 5'-ATAACTTCGTATAGCATACATTATACGAAGTTAT-3' were inserted in the
346 intronic regions flanking the mouse *Dmd* exon 52 (*Dystrophin* NCBI transcript: NM_007868.6) in
347 *C57Bl/6J* mouse ES cells (mES). Positively-targeted mouse ES cells were screened for neomycin
348 cassette (later removed via FRT-mediated recombination) and diphtheria toxin subunit A (DTA)
349 selection. After PCR based confirmation of the presence of the loxP sites and removal of the
350 neomyocin cassette, the resultant ES cell line was injected into pseudopregnant females. The
351 subsequent F_0 offspring were genotyped for presence of the loxP sites at mouse *Dystrophin* exon
352 52, and then positively-targeted males were mated to WT (*C57Bl/6*) females to generate F_1
353 offspring. All positively-targeted F_1 mice were then maintained on the *C57Bl/6* strain for
354 subsequent matings. Mice were genotyped for the *Dmd*$^{flox52/Y}$ allele using a forward primer "5-
355 TGACTGCATCTGCATACGTG-3" and reverse "5-GAAGCCTGGTAGGCACCAT-3". Using the
356 Roche Expand Long Template PCR System (MilliporeSigma; Burlington, MA; Cat# 11681842001)

357 the wild type band (2226 bp), targeted loxP conditional allele (2401 bp), and Cre-mediated
358 excised band (992 bp) were used for genotyping following the manufacturer's recommendations.
359 Later genotyping was performed commercially using Transnetyx probes (Cordova, TN). Isolation
360 of genomic DNA from TA muscles, cerebellum, and tail DNA were performed using Viagen
361 DirectPCR Lysis Reagent (Viagen Biotech; Los Angeles, CA; Cat# 102-T).
362
363 **Histology and Immunofluorescent Imaging**
364 Skeletal muscles were slowly cryofrozen as unfixed tissues in Scigen TissuePlus O.C.T.
365 Compound using an isopentane (FisherScientific; Cat# AC397221000) and liquid nitrogen bath
366 as unfixed tissues. Some muscle biopsies were placed in 30% sucrose (MilliporeSigma; Cat#
367 S0389) sink overnight at 4°C prior to the slow cryofreezing to preserve histological and protein
368 integrity. Muscles were sectioned on a Leica CM1950 cryotome at 7-10 µm thickness, and
369 specimens were placed on Fisherbrand Tissue Path Superfrost Plus Gold slides (Fisher Scientific;
370 Cat# FT4981gplus). H&E staining was performed using Hematoxylin (MilliporeSigma; Cat#
371 H9627) and Eosin Y (MilliporeSigma; Cat# 318906) solutions in a previously described
372 protocol(45). Masson's trichrome staining was performed using a Masson's Trichrome Stain Kit
373 (Polysciences, Inc; Warrington, PA; Cat# 25088-1) and picrosirius red staining was performed
374 using a Picrosirius Red Stain Kit (Polysciences, Inc; Cat# 24901-500). For immunofluorescent
375 staining, tissue slides were blocked for one hour in a solution of 10% goat serum/1xPBS and
376 incubated for one hour at room temperature using a M.O.M kit (Vector Labs; Cat# BMK-2202;
377 Newark, CA). Tissue slides were set using a VECTORSHIELD Antifade mounting medium with
378 DAPI kit (Vector Labs; Cat# H-1200-10),
379
380 **Immunoblotting**
381 Immunoblotting was performed on protein lysates using tissues that were snap frozen in liquid
382 nitrogen and were homogenized using a bead homogenizer and lysing matrix A beads (MP
383 Biomedicals; Cat# 1169100-CF) following the manufacturer's protocol. Samples were
384 homogenized in T-PER™ Tissue Protein Extraction Reagent (ThermoFisher Scientific; Cat#
385 78510) supplemented with a protease inhibitor cocktail (ThermoFisher Scientific; Cat# J61852-
386 XF). Protein lysates were quantified using a Pierce BCA Protein Assay Kit (ThermoFisher
387 Scientific; Cat# 23227), and unless otherwise stated, 50 µg of total whole cell lysate was resolved
388 on 4–20% polyacrylamide Mini-PROTEAN® TGX™ Precast Protein Gels (BioRad). Following an
389 overnight transfer onto PVDF membranes (BioRad; Cat# 1620175), samples were blocked with
390 5% BSA (RPI Corp.; Cat# A30075) and incubated with primary antibody overnight, washed 3

391 times, and incubated with secondary antibodies for 1 hour at room temperature. Membranes were
392 washed 4 times for 15 minutes with gentle rocking, before being incubated with SuperSignal™
393 West Dura Extended Duration Substrate (ThermoFisher Scientific; Cat# 34075). Membranes
394 were imaged on either a ChemiDoc MP Imaging System (BioRad) or a LI-COR Odyssey CLx
395 imager.
396
397 **Antibodies**
398 Primary antibodies used in these experiments were validated on dystrophin-deficient tissues or
399 appropriate control tissues for specificity. Primary antisera used for western immunoblotting and
400 immunofluorescent labeling include: dystrophin all isoforms (Abcam; Cat# ab15277), dystrophin
401 Dys1 (Leica; Cat# NCL-DYS1), and vinculin (Cell Signaling Technology; Cat# 7076S). Secondary
402 antibodies used for western immunoblotting included anti-mouse IgG HRP (Cell Signaling
403 Technology; Cat# 7076S) and anti-rabbit IgG HRP (Cell Signaling Technology; Cat# 7074S).
404 Secondary fluorescent anti-mouse and anti-rabbit IgG fluorochrome-conjugated antibodies used
405 include: Alexa Fluor 488 (ThermoFisher Scientific; Cat# A-11001 and A-11008), Alexa Fluor 555
406 (ThermoFisher Scientific; Cat# A32727 and A32732), and DyLight 633 (ThermoFisher Scientific;
407 Cat# 35563). Fluorescently labeled sections were imaged on a Nikon A1R-HD25 Confocal
408 microscope using NIS Elements software, and later processed using Adobe Photoshop (2025
409 version).
410
411 **Tamoxifen administration**
412 We used a previously-established protocol for the *HSA*-MerCreMer strain of delivering (80 mg/kg
413 body weight) of (Z)-4-hydroxyl-tamoxifen (4-OHT) (MilliporeSigma; Cat# H7904) mixed with
414 sunflower seed oil (MilliporeSigma; Cat# S5007) via 5 daily intraperitoneal injections while
415 alternating left and right sides to avoid injection site reactions (46, 47). Control mice were given
416 equivalent IP injections of sunflower seed oil. Separate mouse cohorts were assessed at 30 day
417 intervals from days 0, 30, 60, 90, and 180 days post injection. Mice were monitored for
418 hepatotoxicity using cytochrome P450 assessments and injection site reactions after
419 administration.
420
421 **Mice locomotor and functional analysis**
422 Open field testing and mouse locomotor analysis was measured using a previously established 4
423 individual chamber sensor system protocol and data was analyzed using Ethovision XT software
424 platform (Noldus; Leesburg, VA)(48, 49). Mice were analyzed for functional analysis but were first

425 acclimated to the room and open-field chambers one day prior to activity and were given a five
426 minute additional adaptation period prior to activity recording. Mouse locomotor activity was
427 recorded for ten minutes with no external stimulation and the experimenter isolated in a separate
428 room.
429
430 **Physiological force assessments**
431 Mice were anesthetized with sodium pentobarbital (80 mg/kg) by intraperitoneal (IP) injection.
432 Isolated EDL muscles were suspended in a phosphate buffer equilibrated with 95% O_2, 5% CO_2
433 (35 °C). Muscle contractions were generated using a 150 ms, supramaximal stimulus train (200
434 μs pulses) with the muscle held at its optimal length (L_o) for tetanic tension. Force was normalized
435 to physiological cross-sectional area assuming a fiber length to muscle length ratio of 0.44 as
436 previously described(32). After evaluation of peak force, muscles were subjected to an active
437 lengthening protocol consisting of the following sequence: one fix-end contraction, 5 lengthening
438 (eccentric) contractions, and two fixed-end contractions. All contractions began with the muscle
439 at L_o and were elicited with 150 ms trains at 300 Hz. The lengthening trials consisted of an initial
440 100 ms fixed-end contraction that allowed the muscle to rise to peak force followed by a constant
441 velocity stretch at four muscle fiber lengths/s to a final length of 120% L_o. Force was evaluated at
442 95 ms of stimulation for both fixed-end and lengthening trials.
443
444 **Social neurobehavior and memory experiments**
445 Social approach was determined by placing the test mouse in the middle chamber of a 3-chamber
446 system and determining if the mouse showed preference for a novel mouse or a novel object
447 (round ball). The social approach protocol was adapted from our previous protocol along with
448 other established mouse neurobehavioral assessments in autism spectrum disorder (ASD)
449 mouse models(20, 50). Mice were evaluated over 10 minute periods after a 10 minute acclimation
450 period in which the novel mouse and novel object were kept in blocked off chambers. Placement
451 of the novel mouse and novel object was switched between the two side chambers between
452 intervals, and the apparatus was cleaned between evaluations. Social novelty was determined by
453 placing the test mouse in the center chamber and evaluating the time spent in chambers
454 containing either an unfamiliar mouse (no previous exposure) or a familiar mouse (aged-matched
455 littermate). The mouse was monitored over a 10 min interval after the 10 minute acclimation
456 period, and its total movement, velocity, time spent in close interaction with familiar or unfamiliar
457 mouse were measured. T-maze and Y-maze (Maze Engineers; Skokie, IL) cohort assessments
458 were performed using previously described with video recordings captured after the mouse was

459 placed in the maze center(51, 52). Spatial memory and learning evaluation of the mouse cohorts
460 was performed using the Morris Water Maze (Noldus) from an adapted protocol previously used
461 in *mdx* mice(53, 54). Experimenter was double-blinded to treatment group and genotype of the
462 mice in each cage and de-blinded occurred after data analysis.
463
464 **Skeletal muscle injury**
465 A cardiotoxin-induced injury to the TA was performed by intramuscular injection of 40 µl of 10 µM
466 cardiotoxin (Millipore Sigma; Cat# 217503) given to adult, aged-matched male mice. The
467 contralateral TA muscle was used as a sham control and given an equivalent intramuscular
468 injection of phosphate-buffered saline (1x DPBS; Millipore Sigma; Cat# D8662) given as a control.
469 Mice were evaluated at day 0 (uninjured), 7, 14, and 21 days post cardiotoxin injury for histological
470 changes in muscle architecture and myofiber composition.
471
472 **RNA-sequencing**
473 Total RNA was extracted from TA skeletal muscles from aged-matched male mice using TRIzol
474 reagent (ThermoFisher Scientific; Cat# 15596026) for extraction following the manufacture's
475 protocol. RNA with an RNA Integrity Score (RIN) greater than 7.0 was selected for library
476 amplification. Poly A enrichment using a ribominus kit (ThermoFisher Scientific; Cat# K155002)
477 was performed on the samples. A total RNA library was amplified from approximately 200-300 ng
478 of RNA using a NovaSeq 6000 reagent kit v1.5 (Illumina; San Diego, CA; Cat# 20044417) before
479 being processed on an Illumina NovaSeq 6000 sequencer. Total reads were FASTQ files were
480 uploaded to the UAB High Performance Computer cluster for bioinformatics analysis with the
481 following custom pipeline built in the Snakemake workflow system (v5.2.2)(55). Following count
482 normalization, principal component analysis (PCA) was performed, and genes were defined as
483 differentially expressed genes (DEGs) if they passed a statistical cutoff containing an adjusted p-
484 value <0.05 (Benjamini-Hochberg False Discovery Rate (FDR) method) and if they contained an
485 absolute $\log_2$ fold change >=1. Functional annotation enrichment analysis was performed in the
486 NIH Database for Annotation, Visualization and Integrated Discovery (DAVID, v6.8) by separately
487 submitting upregulated and downregulated DEGs. Ingenuity pathway analysis (IPA) was
488 performed on the data as described(56). A p-value <0.05 cutoff was applied to identify gene
489 ontology (GO) terms and the FASTQ experimental files have been uploaded to NCBI's Gene
490 Expression Omnibus under accession number GSE284723.
491
492 **Quantitative PCR analysis**

Total RNA was extracted using TRIzol reagent (ThermoFisher Scientific) and the lysing matrix A beads (MP Biomedicals; Cat# 1169100-CF) as described above. Approximately 1 µg of RNA was then reverse transcribed using SuperScript IV First-Strand Synthesis System (ThermoFisher Scientific; Cat# 18091050). Approximately 0.5 µl of sample was then mixed with using TaqMan™ Fast Advanced Master Mix (ThermoFisher; Cat# 4444556) following the manufacturer's protocol and samples were analyzed on a QuantStudio 5 Real-Time PCR machine (ThermoFisher). The following Taqman real time PCR assays (ThermoFisher Scientific) were used to amplify specific transcripts: *Dmd* (exon 1, Mm03956078_s1; exons 16-17, Mm00464475_m1; exons 50-51, Mm01216958_m1; exons 64-65, Mm00464520_m1), and *Actb1* (Mm02619580_g1).

Statistical Analysis

For most dual cohort comparisons, either a two-tailed student's t-test or chi-squared test for normality was performed for all pairwise comparisons. For longitudinal assessments over time or across multiple cohorts, a one-way analysis of variance (ANOVA) with Least Significant Difference (LSD) was performed for all multiple comparisons. GraphPad Prism version 10 software (Graphpad Software; San Diego, CA) was used for all statistical analyses. An *a priori* hypothesis of *$p< 0.05$, **$p<0.01$, ***$p<0.001$, and ****$p< 0.0001$ was used for all reported data analyses. All graphs were represented as mean +/- SEM.

Acknowledgments and Funding

We would like to thank members of the Alexander lab and UAB Center for Exercise Medicine for their critical evaluation of our manuscript. We would also like to thank members of the Kunkel, Gamble, and Esser labs for reviewing our manuscript and assistance with data interpretation. M.S.A. is supported by NIH grants from the Office of the Director under award number (U54OD030167), and an R21 grant from National Institute of Neurological Disorders and Stroke (NINDS) (R21NS140497). Additional funding support was provided by the Hope4Gabe foundation. L.M.K. is supported by NIH National Institute of Arthritis and Musculoskeletal and Skin Diseases (NIAMS) grant R01AR064300, and the Bernard F. and Alva B. Gimbel Foundation. K.L.G. is funded by an NIH National Institute on Drug Abuse (NIDA) grants R01DA046096 and R01NS082413. K.A.E. is funded by NIH NIAMS grants (R01AR066082 and R01AR079220). M.A.L. is supported by an NIH NIAMS grant K08NS120812.

Figure Legends

527

528 **Figure 1. Characterization of a myofiber-specific *Dmd* conditional knockout mouse. A.**
529 Schematic outlining the generation of myofiber-specific Dystrophin conditional knockout mice
530 (*Dmd*:HSA KO) by breeding our $Dmd^{flox52/Y}$ mice to human skeletal actin (*HSA*)-Cre transgenic
531 mice. Cre-mediated excision of *Dmd* exon 52 results in an out-of-frame disruption and instability
532 of the Dp427 RNA transcript. **B.** Western immunoblotting for the large Dp427m protein in the TA
533 and soleus muscles of WT (open), $Dmd^{flox52/Y}$ (blue), mdx^{5cv} (red), and *Dmd*:HSA KO (green) adult
534 (6-month-old) male mice. **C.** Densitometry graphs WT, $Dmd^{flox52/Y}$, mdx^{5cv}, and *Dmd*:HSA KO
535 immunoblots taken from TA and soleus muscle lysates and normalized to Vinculin protein. N = 5
536 separate mice per cohort. **D.** Histochemical staining of TA, soleus, and diaphragm muscles
537 isolated from the WT, $Dmd^{flox52/Y}$, mdx^{5cv}, and *Dmd*:HSA KO male mice. Hematoxylin and eosin
538 (H&E), picrosirius red, and Masson's trichrome histochemical staining performed. Scale bar = 100
539 µm. **E.** Percent fibrosis (%) in the TA muscles of the four mouse cohorts analyzed. **F.** Percentage
540 (%) centralized myonuclei for the approximately 600 myofibers of the TA muscles of the four
541 mouse cohorts analyzed. **G.** Cross-sectional area (CSA) displaying myofiber sizes (μm^2) shown
542 for each of the four cohorts. Two-way ANOVA with Bonferroni correction performed. P-values of
543 significance are shown: * $p < 0.05$, ** $p < 0.01$, *** $p < 0.005$, and **** $p < 0.001$.
544

545 **Figure 2. Adult *Dmd* myofiber KO mice have a poor running capacity. A.** Rotarod analysis
546 shown for the four mouse cohorts: WT, $Dmd^{flox52/Y}$, mdx^{5cv}, and *Dmd*:HSA KO. **B.** Grip strength
547 measured for mouse forelimbs shown normalized to grams (g) body weight. **C.** Open field testing
548 (OFT) of the four cohorts of mice showing distance traveled in centimeters (cm). **D.** and **E.** Forced
549 downhill treadmill running of the four cohorts of mice with average velocity and time to exhaustion
550 shown. N = 6 mice/cohort. Two-way ANOVA with Bonferroni correction performed. P-values of
551 significance are shown: * $p < 0.05$, ** $p < 0.01$, *** $p < 0.005$, and **** $p < 0.001$.
552

553 **Figure 3. *Dmd* myofiber KO muscles have disrupted cytokine and ECM signaling pathways.**
554 **A.** Volcano plot of the approximately 6,200 dysregulated DEGs in the TA muscles of *Dmd*:HSA
555 KO mice compared to $Dmd^{flox52/Y}$ (HSA-Cre-negative) aged-matched littermate controls. **B.** and **C.**
556 Heatmaps of significantly dysregulated showing significantly elevated (> 2.0 fold) or
557 downregulated (< 2.0 blue) DEGs with an emphasis on cytokine and ECM pathways. D. RNA-seq
558 DeSeq2 FKPM counts of three candidate highly disrupted transcripts that are validated DMD
559 muscle biomarkers: *Nos2*, *Col4a4*, and *Tgfb1* are shown. Four mice of each cohort ($Dmd^{flox52/Y}$-
560 black; *Dmd*:HSA KO- red) were analyzed for differentially expressed genes (DEGs). Student's t-

561 test, two tailed used for comparisons. P-values of significance are shown: * $p < 0.05$, ** $p < 0.01$,
562 *** $p < 0.005$, and **** $p < 0.001$.
563
564 **Figure 4. Postnatal loss of muscle dystrophin results in mild skeletal muscle pathologies.**
565 **A.** Schematic for conditional ablation of postnatal dystrophin using a tamoxifen-inducible (± TAM)
566 strategy. *Dmd*$^{flox52/Y}$ mice were mated to the *HSA*-MerCreMer (HSA-MCM) to conditionally ablate
567 dystrophin (+ TAM; red). *Dmd*:HSA (Cre+) mice given sunflower seed oil (- TAM) were used as
568 controls (black) After a one-week (5x per week) tamoxifen dosing (80 mg/kg body weight) in 8-
569 week-old male mice via intraperitoneal injection, mouse cohorts were evaluated at 0 (pre-dosing),
570 30, 60, 90, and 180 days (d) post deletion. N = 5 mice per cohort and time period for biopsy. **B.**
571 Densitometry western immunoblot measurements of the large dystrophin (Dp427m) protein
572 isoform measured in the TA, soleus, and diaphragm muscles. Note the robust persistence of the
573 large dystrophin protein and low protein turnover in the skeletal muscle tissues. **C.** H&E evaluation
574 of *Dmd*$^{flox52/Y}$:HSA-MCM (Cre+) mice (± TAM) evaluated at 180 days post ablation. Scale bar =
575 200 µm. **D.** and **E.** CSA and minimum Feret diameter measured at 180 days in the TA muscles
576 reveal smaller groupings of myofibers in the *md*$^{flox52/Y}$:HSA-MCM (Cre+) mice (+ TAM) mice
577 compared to (- TAM) controls. Student's t-test, two tailed used for comparisons. P-values of
578 significance are shown: * $p < 0.05$, ** $p < 0.01$, *** $p < 0.005$, and **** $p < 0.001$.
579
580 **Figure 5. Loss of Purkinje neuron brain *Dystrophin* impairs neurobehaviors in mice. A.**
581 Breeding schematic for the *Dmd*$^{flox52/Y}$ line to the *L7/Pcp2*-Cre (cerebellar Cre driver) transgenic
582 line to generate Dmd:Pcp2 KO mice. **B.** Densitometry western immunoblot quantification of the
583 large dystrophin (Dp427) protein expression in the cerebellum, cortex, and hypothalamus regions
584 of the brain in the *Dmd*$^{flox52/Y}$ (Cre-; open) and *Dmd*:Pcp2 KO (Cre+; grey) cohorts. N = 5 mice per
585 cohort were analyzed. **C.** Graphics showing the social approach (novel mouse versus novel
586 object) and social novelty (novel mouse versus familiar mouse) assays performed on the cohorts
587 of mice in a 3-chamber assay system. **D.** and **E.** Social approach and social novelty time in
588 chambers (1, 2, and 3) shown between the 3 analyzed mouse cohorts: the *Dmd*$^{flox52/Y}$ (open bars),
589 *Dmd*:Pcp2 KO (grey bars), and *mdx*^{5cv} (red bars). Time in chamber and time investigating in
590 minutes (mins) are shown. N = 10 mice per cohort were analyzed with an acclimation period of
591 equivalent amounts. **F.** and **G.** T- and Y-maze assessments of the 3 mouse cohorts are shown
592 with spontaneous alternation and the number of total arm visits. **H.** Morris water maze (MWM)
593 assessments in the 3 cohorts are shown as distance to platform (cm) compared to trial day. Spatial
594 and reverse learning assessments were performed on separate days. N = 10 adult (6-month-old)

mice were analyzed for each cohort. Two-way ANOVA with Bonferroni correction performed. P-values of significance are shown: * $p < 0.05$, ** $p < 0.01$, *** $p < 0.005$, and **** $p < 0.001$.

Supplementary Figure Legend

Supplemental Figure S1: Immunofluorescent confirmation of the loss of skeletal muscle dystrophin. Immunofluorescent imaging of the TA skeletal muscle and the DYS1 (Dp427 large isoform; purple) along with laminin (green) and DAPI (blue nuclei) co-labeling. Each of the four mouse cohorts are represented: WT, *Dmd*$^{flox52/Y}$, *mdx*^{5cv}, and *Dmd*:HSA KO. Scale bar = 100 µm. N = 5 adult (6-month-old) mice were analyzed for each cohort.

Supplemental Figure S2: Adult *Dmd* myofiber KO mice have physiological force deficits. A. Mass (mg) of muscles from *Dmd*^{flox52}/Y (Cre-) (black) and *Dmd*$^{flox52/Y}$:HSA KO (Cre+) (red) mice. **B.** Absolute peak muscle force (mN). **C.** Peak muscle force normalized to CSA (kPa). **D.** Fix-end force during the eccentric contraction protocol. Force expressed relative to the force attained on the initial fixed end contraction. **E.** Post eccentric relative force (mN). N = 10 mice per cohort. One-way ANOVA with Bonferroni correction is shown. P-values of significance are shown: * $p < 0.05$, ** $p < 0.01$, *** $p < 0.005$, and **** $p < 0.001$; ns = non-significant.

Supplemental Figure S3: Conditional *Dmd* myofiber KO mice have impaired skeletal muscle regeneration. A. Histochemical evaluation of the TA muscles 14 and 21 days post cardiotoxin-induced skeletal muscle injury. H&E, picrosirius red, and Masson's trichrome staining of the TA muscles showing elevated areas of fibrosis, myofiber degeneration, and necrosis in the *Dmd*:HSA mKO mice at 14d and 21d post-ctx induced muscle injury compared to *Dmd*$^{flox52/Y}$ control mice. Scale bar = 100 µm. **B.** Laminin immunofluorescent imaging showing increased centralized myonuclei and smaller myofibers in the 14d and 21d post-ctx injured *Dmd*:HSA mKO mice. Scale bar = 80 µm. N = 5 mice per cohort.

Supplemental Figure S4: IPA pathway analysis of the conditional *Dmd* myofiber knockout mice. IPA analysis of the top dysregulated signaling pathways disrupted in the adult TA muscles of the *Dmd*:HSA mKO mice compared to *Dmd*$^{flox52/Y}$ control mice. -log p-values shown with increased pathways (orange) and downregulated pathways (blue) shown.

628 **Supplemental Figure S5: Confirmation of cerebellar dystrophin Dp427 protein knockdown**
629 **in Dmd:Pcp2 isolated cerebellums.** Western immunoblot analysis showing knockdown of
630 cerebellar large dystrophin (Dp427c) in the isolated cerebellums of adult *Dmd*:Pcp2 KO mice. WT
631 (*C57BL/6J*), $Dmd^{flox52/Y}$, and *Dmd*:Pcp2 KO mouse cohorts were analyzed. The Dp140 dystrophin
632 isoform was also reduced in the *Dmd*:Pcp2 KO mouse cohorts. GAPDH levels were used to
633 normalize protein lysates for comparative analyses.
634
635 **References**
636

637 1. M. Koenig.et.al¡, Complete cloning of the duchenne muscular dystrophy (DMD) cDNA and
638 preliminary genomic organization of the DMD gene in normal and affected individuals. Cell
639 50, 509-517 (1987).
640 2. E. P. Hoffman, R. H. Brown, L. M. Kunkel, Dystrophin: the protein product of the Duchenne
641 muscular dystrophy locus. Cell 51, 919 - 928 (1987).
642 3. G. Bulfield, W. G. Siller, P. A. Wight, K. J. Moore, X chromosome-linked muscular dystrophy
643 (mdx) in the mouse. Proceedings.of.the.National.Academy.of.Sciences 81, 1189-1192
644 (1984).
645 4. P. Sicinski.et.al¡, The molecular basis of muscular dystrophy in the mdx mouse: a point
646 mutation. Science 244, 1578-1580 (1989).
647 5. M. Rodrigues, Y. Echigoya, S.-i. Fukada, T. Yokota, Current Translational Research and
648 Murine Models For Duchenne Muscular Dystrophy. J.Neuromuscul.Dis 3, 29-48 (2016).
649 6. A. Bez Batti Angulski.et.al¡, Investigations of an inducible intact dystrophin gene excision
650 system in cardiac and skeletal muscle in vivo. Scientific.Reports 10, 10967 (2020).
651 7. E. Araki.et.al¡, Targeted Disruption of Exon 52 in the Mouse Dystrophin Gene Induced Muscle
652 Degeneration Similar to That Observed in Duchenne Muscular Dystrophy. Biochemical.and.
653 Biophysical.Research.Communications 238, 492-497 (1997).
654 8. A. Saoudi.et.al¡, Emotional behavior and brain anatomy of the mdx52 mouse model of
655 Duchenne muscular dystrophy. Disease.Models.™ .Mechanisms 14 (2021).
656 9. S. Shibuya.et.al¡, Muscle Plasma Membrane Changes in Dystrophin Gene Exon 52 Knockout
657 Mouse. Pathology._.Research.and.Practice 197, 441-447 (2001).
658 10. T. Oliver.et.al¡, The glucocorticoid receptor acts locally to protect dystrophic muscle and
659 heart during disease. Disease.Models.™ .Mechanisms 17 (2024).
660 11. C. Vaillend.et.al¡, Duchenne muscular dystrophy: recent insights in brain related
661 comorbidities. Nature.Communications 16, 1298 (2025).
662 12. A. Saoudi.et.al¡, Impact of distinct dystrophin gene mutations on behavioral phenotypes of
663 Duchenne muscular dystrophy. Disease.Models.™ .Mechanisms 17 (2024).
664 13. Y. Hashimoto.et.al¡, Brain Dp140 alters glutamatergic transmission and social behaviour in
665 the mdx52 mouse model of Duchenne muscular dystrophy. Progress.in.Neurobiology 216,
666 102288 (2022).
667 14. N. Beastrom.et.al¡, mdx5cv Mice Manifest More Severe Muscle Dysfunction and Diaphragm
668 Force Deficits than Do mdx Mice. The.American.Journal.of.Pathology 179, 2464-2474 (2011).
669 15. R. Willmann.et.al¡, Enhancing translation: Guidelines for standard pre-clinical experiments
670 in mdx mice. Neuromuscular.Disorders 22, 43-49 (2012).

16. K. E. Wells.et.al¡, Relocalization of neuronal nitric oxide synthase (nNOS) as a marker for complete restoration of the dystrophin associated protein complex in skeletal muscle. Neuromuscular.Disorders 13, 21-31 (2003).
17. Y. Lai.et.al¡, Dystrophins carrying spectrin-like repeats 16 and 17 anchor nNOS to the sarcolemma and enhance exercise performance in a mouse model of muscular dystrophy. The.Journal.of.Clinical.Investigation 119, 624-635 (2009).
18. J. A. Call, J. N. Mckeehen, S. A. Novotny, D. A. Lowe, Progressive resistance voluntary wheel running in the mdx mouse. Muscle.™ .Nerve 42, 871-880 (2010).
19. K. E. Schill.et.al¡, Muscle damage, metabolism, and oxidative stress in mdx mice: Impact of aerobic running. Muscle.™ .nerve 54, 110-117 (2016).
20. M. S. Alexander.et.al¡, Reversal of neurobehavioral social deficits in dystrophic mice using inhibitors of phosphodiesterases PDE5A and PDE9A. Translational.Psychiatry 6, e901-e901 (2016).
21. M. E. D. Stefano, V. Ferretti, C. Mozzetta, Synaptic alterations as a neurodevelopmental trait of Duchenne muscular dystrophy. Neurobiology.of.Disease 168, 105718 (2022).
22. C. Vaillend, R. Chaussenot, Relationships linking emotional, motor, cognitive and GABAergic dysfunctions in dystrophin-deficient mdx mice. Human.Molecular.Genetics 26, 1041-1055 (2017).
23. J. W. McGreevy, C. H. Hakim, M. A. McIntosh, D. Duan, Animal models of Duchenne muscular dystrophy: from basic mechanisms to gene therapy. Disease.Models.™ . Mechanisms 8, 195-213 (2015).
24. C. R. Heier.et.al¡, The X-linked Becker muscular dystrophy (bmx) mouse models Becker muscular dystrophy via deletion of murine dystrophin exons 45–47. Journal.of.Cachexia? Sarcopenia.and.Muscle 14, 940-954 (2023).
25. M. Ghahramani Seno.et.al¡, Transcriptomic analysis of dystrophin RNAi knockdown reveals a central role for dystrophin in muscle differentiation and contractile apparatus organization. BMC.Genomics 11, 345 (2010).
26. M. R. F. Gosselin.et.al¡, Loss of full-length dystrophin expression results in major cell-autonomous abnormalities in proliferating myoblasts. eLife 11, e75521 (2022).
27. In Y. Choi.et.al¡, Concordant but Varied Phenotypes among Duchenne Muscular Dystrophy Patient-Specific Myoblasts Derived using a Human iPSC-Based Model. Cell.Reports 15, 2301-2312 (2016).
28. L. Caputo.et.al¡, Acute conversion of patient-derived Duchenne muscular dystrophy iPSC into myotubes reveals constitutive and inducible over-activation of TGFβ-dependent pro-fibrotic signaling. Skeletal.Muscle 10, 13 (2020).
29. J. Massenet.et.al¡, Epigenetic control of myogenic identity of human muscle stem cells in Duchenne Muscular Dystrophy. bioRxiv 10.1101/2023.04.26.538414, 2023.2004.2026.538414 (2023).
30. Y. Liu.et.al¡, PTPN1/2 inhibition promotes muscle stem cell differentiation in Duchenne muscular dystrophy. Life.Science.Alliance 8, e202402831 (2025).
31. F. Yue.et.al¡, PTEN Inhibition Ameliorates Muscle Degeneration and Improves Muscle Function in a Mouse Model of Duchenne Muscular Dystrophy. Molecular.Therapy 29, 132-148 (2021).
32. M. S. Alexander.et.al¡, MicroRNA-486–dependent modulation of DOCK3/PTEN/AKT signaling pathways improves muscular dystrophy–associated symptoms. The.Journal.of.Clinical. Investigation 124, 2651-2667 (2014).
33. N. A. Dumont.et.al¡, Dystrophin expression in muscle stem cells regulates their polarity and asymmetric division. Nat.Med 21, 1455-1463 (2015).

34. Y. X. Wang.et.al¡, EGFR-Aurka Signaling Rescues Polarity and Regeneration Defects in Dystrophin-Deficient Muscle Stem Cells by Increasing Asymmetric Divisions. Cell.Stem.Cell 10.1016/j.stem.2019.01.002 (2019).
35. K. Kodippili, M. A. Rudnicki, Satellite cell contribution to disease pathology in Duchenne muscular dystrophy. Frontiers.in.Physiology 14 (2023).
36. U. Gurriaran-Rodriguez.et.al¡, Wnt7a is Required for Regeneration of Dystrophic Skeletal Muscle. bioRxiv 10.1101/2024.01.24.577041, 2024.2001.2024.577041 (2024).
37. C. Pascual-Morena.et.al¡, Dystrophin Genotype and Risk of Neuropsychiatric Disorders in Dystrophinopathies: A Systematic Review and Meta-Analysis. J.Neuromuscul.Dis 10, 159-172 (2023).
38. M. Thangarajh.et.al¡, Relationships between DMD mutations and neurodevelopment in dystrophinopathy. Neurology 93, e1597-e1604 (2019).
39. M. Thangarajh.et.al¡, Neurodevelopmental Needs in Young Boys with Duchenne Muscular Dystrophy (DMD): Observations from the Cooperative International Neuromuscular Research Group (CINRG) DMD Natural History Study (DNHS). PLoS.currents 10, ecurrents.md.4cdeb6970e54034db54032bc54033dfa54054b54034d54987 (2018).
40. W.-C. Wu, S. P. Bradley, J. M. Christie, J. R. Pugh, Mechanisms and Consequences of Cerebellar Purkinje Cell Disinhibition in a Mouse Model of Duchenne Muscular Dystrophy. The.Journal.of.Neuroscience 42, 2103-2115 (2022).
41. T. L. Stay, L. N. Miterko, M. Arancillo, T. Lin, R. V. Sillitoe, In vivo cerebellar circuit function is disrupted in an mdx mouse model of Duchenne muscular dystrophy. Disease.Models.™. Mechanisms 10.1242/dmm.040840, dmm.040840 (2019).
42. R. Chaussenot.et.al¡, Cognitive dysfunction in the dystrophin-deficient mouse model of Duchenne muscular dystrophy: A reappraisal from sensory to executive processes. Neurobiology.of.Learning.and.Memory 124, 111-122 (2015).
43. F. Zarrouki.et.al¡, Partial Restoration of Brain Dystrophin and Behavioral Deficits by Exon Skipping in the Muscular Dystrophy X-Linked (mdx) Mouse. Annals.of.Neurology 92, 213-229 (2022).
44. C. Vaillend.et.al¡, Rescue of a Dystrophin-like Protein by Exon Skipping In Vivo Restores GABAA-receptor Clustering in the Hippocampus of the mdx Mouse. Mol.Ther 18, 1683-1688 (2010).
45. C. Wang, F. Yue, S. Kuang, Muscle Histology Characterization Using H&E Staining and Muscle Fiber Type Classification Using Immunofluorescence Staining. Bio.Protoc 7 (2017).
46. L. A. Riley.et.al¡, The skeletal muscle circadian clock regulates titin splicing through RBM20. eLife 11, e76478 (2022).
47. B. D. Harfmann.et.al¡, Muscle-specific loss of Bmal1 leads to disrupted tissue glucose metabolism and systemic glucose homeostasis. Skeletal.Muscle 6, 12 (2016).
48. A. L. Reid.et.al¡, DOCK3 is a dosage-sensitive regulator of skeletal muscle and Duchenne muscular dystrophy-associated pathologies. Human.Molecular.Genetics 29, 2855-2871 (2020).
49. Y. M. Kobayashi, E. P. Rader, R. W. Crawford, K. P. Campbell, Endpoint measures in the mdx mouse relevant for muscular dystrophy pre-clinical studies. Neuromuscular.Disorders 22, 34-42 (2012).
50. M. Yang, J. L. Silverman, J. N. Crawley, "Automated Three-Chambered Social Approach Task for Mice" in Current Protocols in Neuroscience. (John Wiley & Sons, Inc., 2011).
51. C. Vaillend, A. Rendon, R. Misslin, A. Ungerer, Influence of dystrophin-gene mutation on mdx mouse behavior. I. Retention deficits at long delays in spontaneous alternation and bar-pressing tasks. Behav.Genet 25, 569-579 (1995).

52. S. Engelbeen, A. Aartsma-Rus, B. Koopmans, M. Loos, M. van Putten, Assessment of Behavioral Characteristics With Procedures of Minimal Human Interference in the mdx Mouse Model for Duchenne Muscular Dystrophy. Frontiers.in.Behavioral.Neuroscience 14 (2021).
53. M. Verhaeg.et.al¡, Learning, memory and blood–brain barrier pathology in Duchenne muscular dystrophy mice lacking Dp427, or Dp427 and Dp140. Genes?.Brain.and.Behavior 23, e12895 (2024).
54. C. V. Vorhees, M. T. Williams, Morris water maze: procedures for assessing spatial and related forms of learning and memory. Nature.Protocols 1, 848-858 (2006).
55. J. Köster, S. Rahmann, Snakemake—a scalable bioinformatics workflow engine. Bioinformatics 28, 2520-2522 (2012).
56. A. Krämer, J. Green, J. Pollard, S. Tugendreich, Causal analysis approaches in Ingenuity Pathway Analysis. Bioinformatics 30, 523-530 (2014).

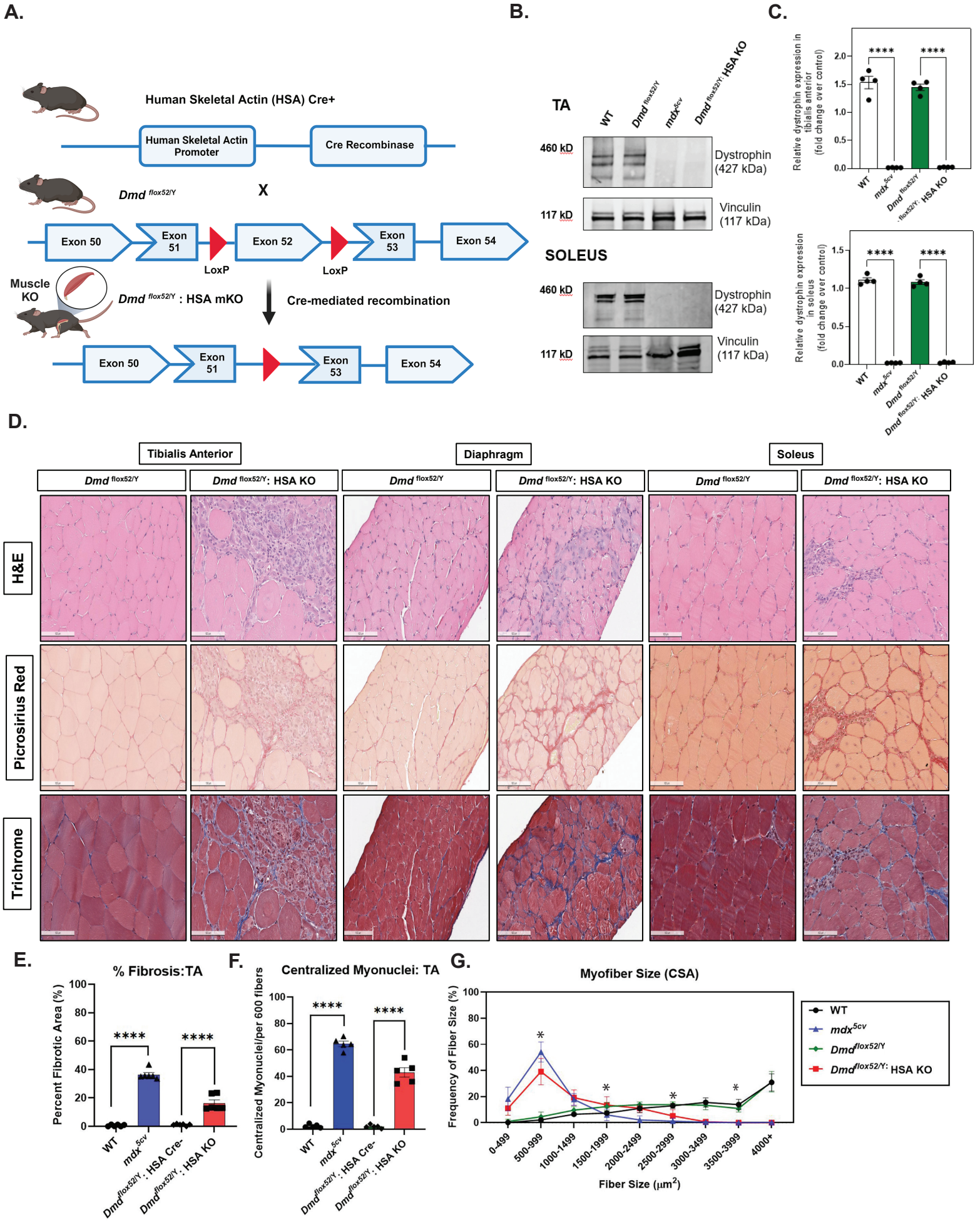

Figure 1. Characterization of a myofiber-specific *Dmd* conditional Dmd knockout mouse.

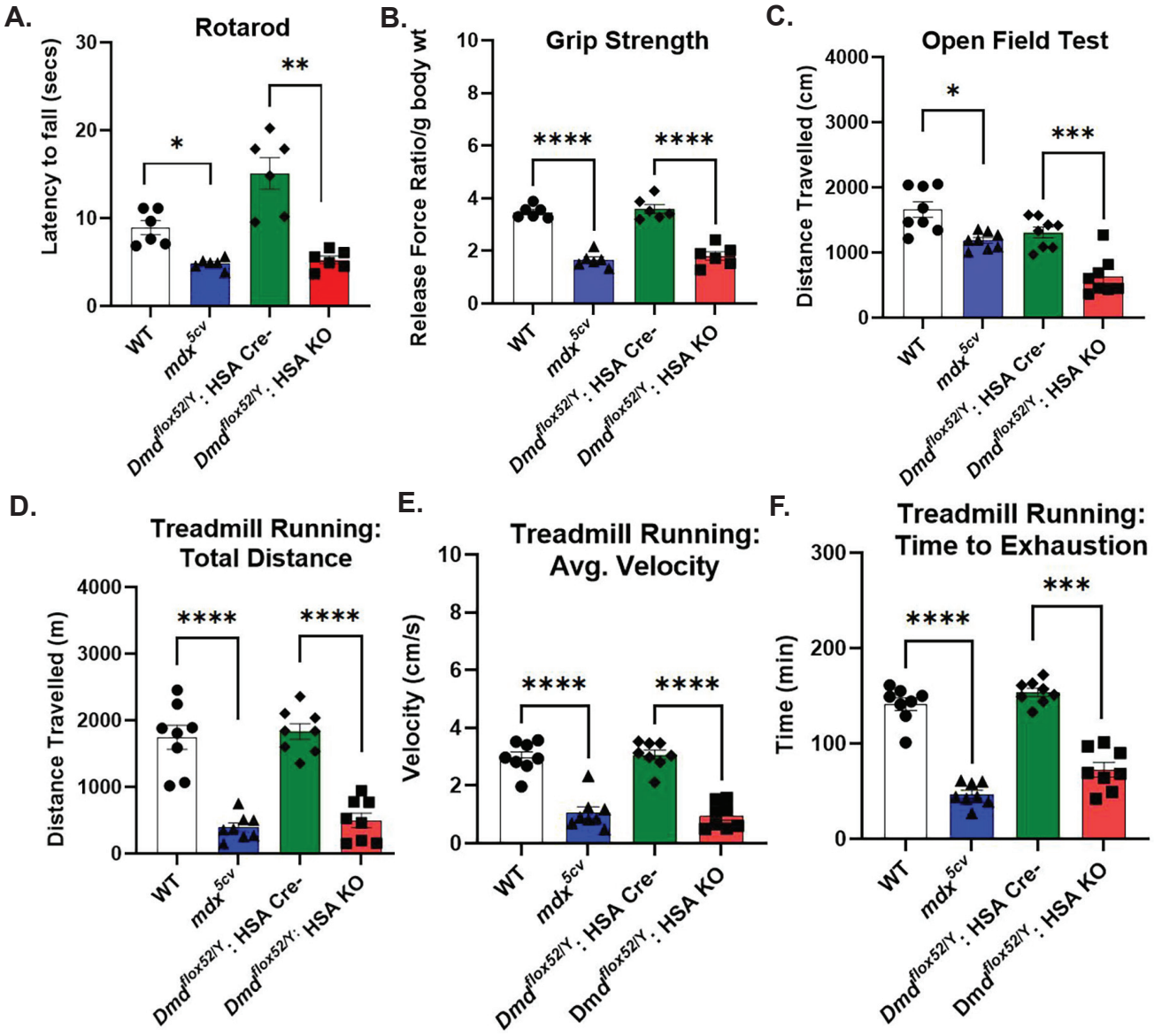

Figure 2: Adult *Dmd* myofiber KO mice have a poor running capacity.

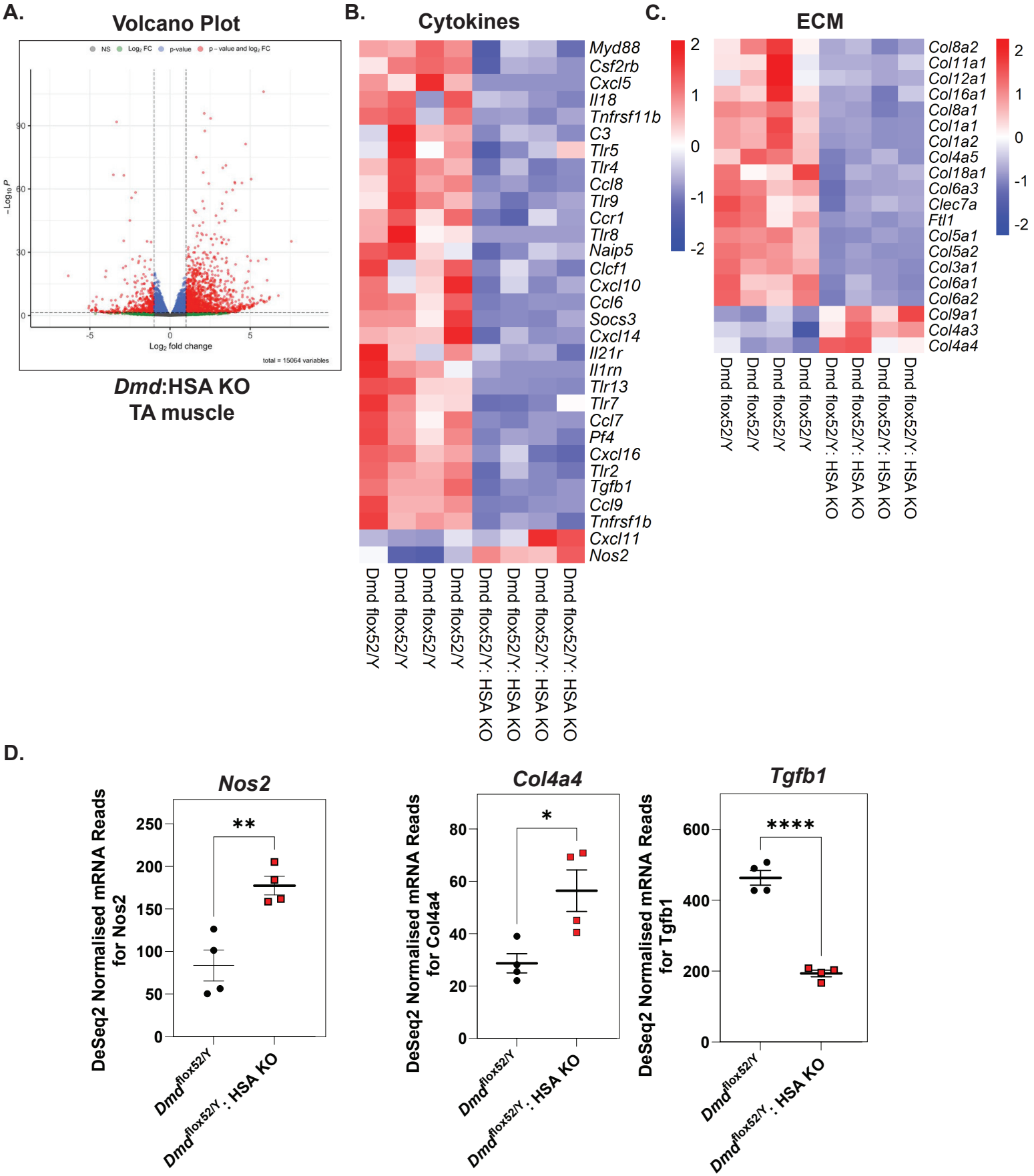

Figure 3: *Dmd* myofiber KO muscles have disrupted cytokine and ECM signaling pathways.

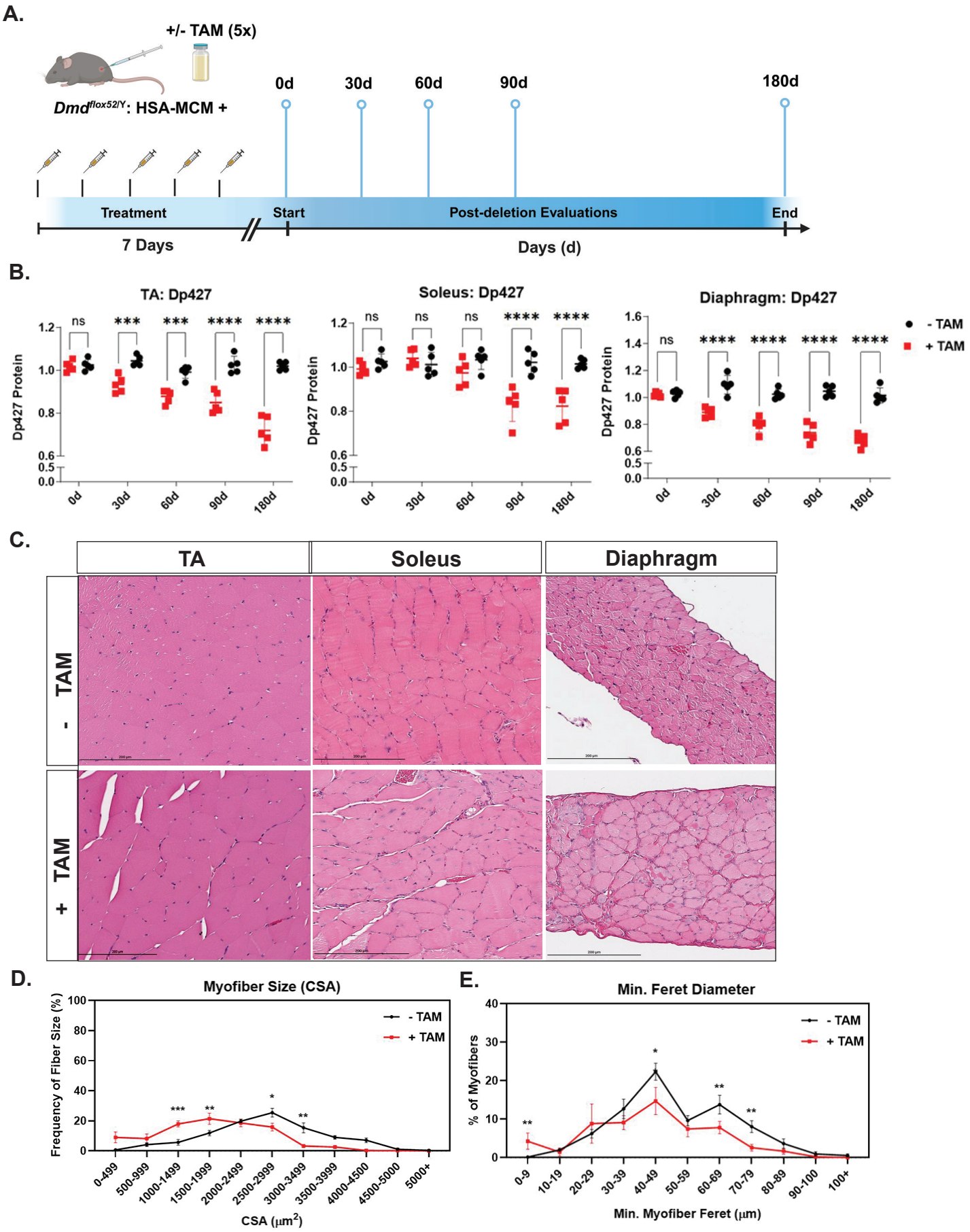

Figure 4. Postnatal loss of muscle dystrophin results in a mild skeletal muscle pathologies.

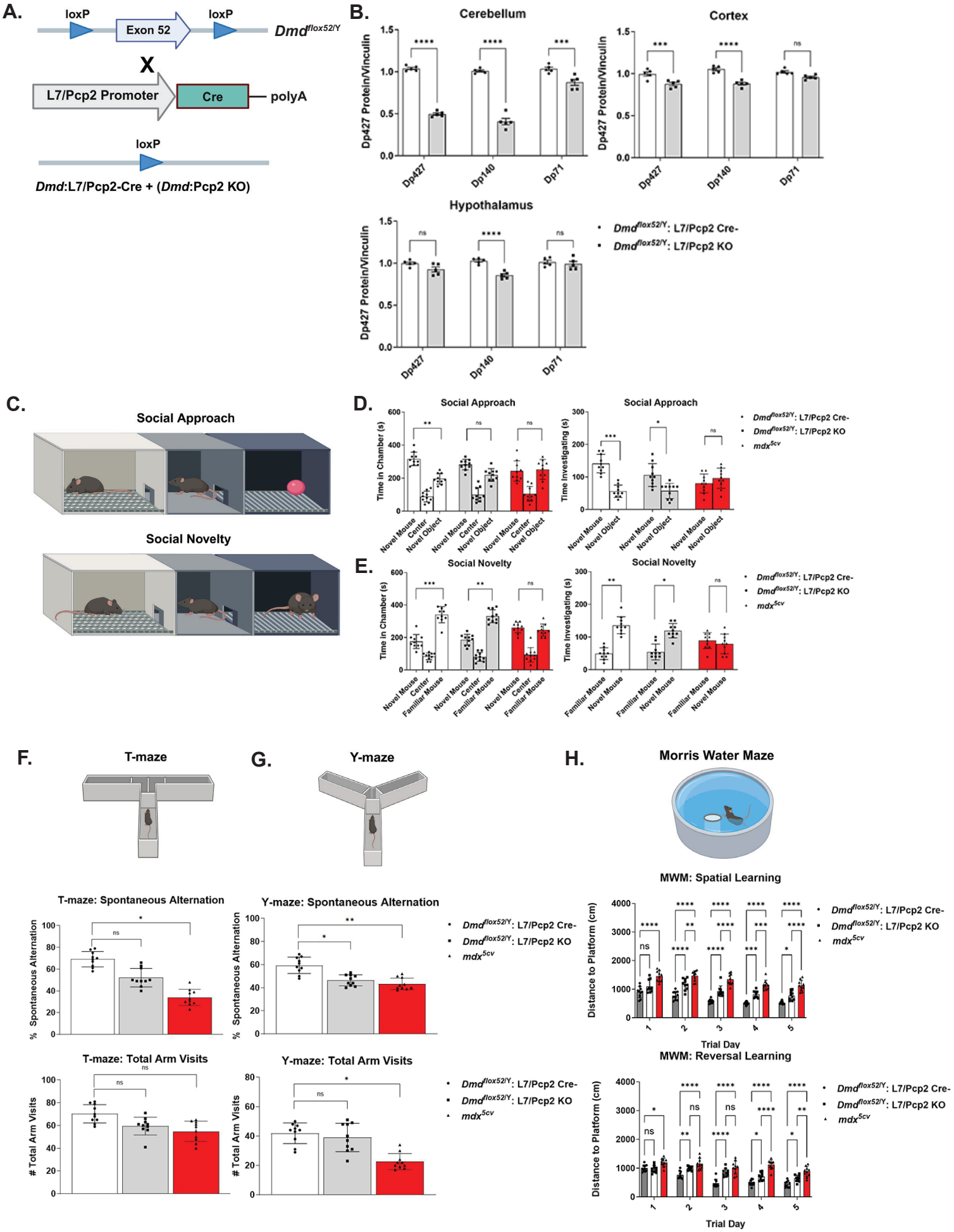

Figure 5. Loss of Purkinje neuron brain *Dystrophin* impairs neurobehaviors in mice.